Inorganic Chemistry
Article

Inorg. Chem. **2010**, *49*, 8779–8789 **8779**
DOI: 10.1021/ic100814j

Synthesis, X-ray Structure, Magnetic Resonance, and DFT Analysis of a Soluble Copper(II) Phthalocyanine Lacking C−H Bonds†

Hans Moons,‡ Łukasz Łapok,§ Andrei Loas,§ Sabine Van Doorslaer,*,‡ and Sergiu M. Gorun*,§

‡*SIBAC Laboratory, Department of Physics, University of Antwerp, Universiteitsplein 1, 2610 Wilrijk, Belgium, and* §*Department of Chemistry and Environmental Science, New Jersey Institute of Technology, Newark, New Jersey 07102*

Received April 26, 2010

The synthesis, crystal structure, and electronic properties of perfluoro-isopropyl-substituted perfluorophthalocyanine bearing a copper atom in the central cavity (F_{64}PcCu) are reported. While most halogenated phthalocyanines do not exhibit long-term order sufficient to form large single crystals, this is not the case for F_{64}PcCu. Its crystal structure was determined by X-ray analysis and linked to the electronic properties determined by electron paramagnetic resonance (EPR). The findings are corroborated by density functional theory (DFT) computations, which agree well with the experiment. X-band continuous-wave EPR spectra of undiluted F_{64}PcCu powder, indicate the existence of isolated metal centers. The electron-withdrawing effect of the perfluoroalkyl (R_f) groups significantly enhances the complexes solubility in organic solvents like alcohols, including via their axial coordination. This coordination is confirmed by X-band ^{1}H HYSCORE experiments and is also seen in the solid state via the X-ray structure. Detailed X-band CW-EPR, X-band Davies and Mims ENDOR, and W-band electron spin-echo-detected EPR studies of F_{64}PcCu in ethanol allow the determination of the principal *g* values and the hyperfine couplings of the metal, nitrogen, and fluorine nuclei. Comparison of the *g* and metal hyperfine values of F_{64}PcCu and other PcCu complexes in different matrices reveals a dominant effect of the matrix on these EPR parameters, while variations in the ring substituents have only a secondary effect. The relatively strong axial coordination occurs despite the diminished covalency of the C−N bonds and potentially weakening Jahn−Teller effects. Surprisingly, natural abundance ^{13}C HYSCORE signals could be observed for a frozen ethanol solution of F_{64}PcCu. The ^{13}C nuclei contributing to the HYSCORE spectra could be identified as the pyrrole carbons by means of DFT. Finally, ^{19}F ENDOR and easily observable paramagnetic NMR were found to relate well to the DFT computations, revealing negligible isotropic hyperfine (Fermi contact) contributions. The single-site isolation in solution and solid state and the relatively strong coordination of axial ligands, both attributed to the introduction of R_f groups, are features important for materials and catalyst design.

Introduction

Phthalocyanines (Pc's) and metal phthalocyanines (PcM's) have many applications, such as dyes and pigments, liquid crystals, photodynamic therapy, nonlinear optical materials, semiconductors and photovoltaics, gas sensors, and catalytic materials.[1] Different parameters are known to influence the characteristics of metallophthalocyanines, including variations in both the organic ligand and the metal center. About 70 different metal ions can be placed in or above the central cavity of Pc's leading to materials with different properties that can be further varied by axial ligands. Planar phthalocyanines are known to aggregate via $\pi-\pi$ stacking interactions or single-atom bridges, largely hampering solubility or single-site accessibility, important in catalysis. The steric and electronic features of phthalocyanines can, however, be tuned by their ring substituents. The formation of monomeric species with potential catalytic and photocatalytic reactivity is, in principle, facilitated by the use of bulky, peripheral substituents. Among electron-poor phthalocyanines, the electron-withdrawing halogen substituents in X_{16}Pc (X = F, Cl, Br) lead to electronic deficiency but also to poor solubility in organic solvents.

Some of us have shown recently that the introduction of eight *i*-C_3F_7 peripheral substituents in the perfluorophthalocyanine ring results in the facile formation of 29*H*, 31*H*,1,4,8,11,15,18,22,25-octafluoro-2,3,9,10,16,17,23,24-octakisperfluoro(isopropyl) phthalocyanine, $F_{64}PcH_2$,[2,3] and its zinc and cobalt complexes[4−6] (Figure 1a). This new class of

† Dedicated to Prof. Stephen J. Lippard on the occasion of his 70th birthday.

*To whom correspondence should be addressed. E-mail: sabine.vandoorslaer@ua.ac.be (S.V.D), gorun@njit.edu (S.M.G.).

(1) (a) McKeown, N. B. *Phthalocyanine Materials: Synthesis, Structure and Function*; Cambridge University Press: Cambridge, U.K., 1998. (b) *Phthalocyanines: Properties and Applications*; Leznoff, C. C., Lever, A. B. P., Eds.; VCH publishers: New York, 1990−1996; Vols. *1*−*4*. (c) Gerdes, R.; Lapok, L.; Tsaryova, D.; Woehrle, D.; Gorun, S. M. *Dalton Trans.* **2009**, 1098–1100. (d) Gorun, S. M.; Rathke, J. W.; Chen, M. J. *Dalton Trans.* **2009**, 1095–1097.

(2) Lee, H.-J.; Brennessel, W. W.; Lessing, J. A.; Brucker, W. W.; Young, V. G., Jr.; Gorun, S. M. *Chem. Commun.* **2003**, 1576–1577.

Published on Web 09/03/2010

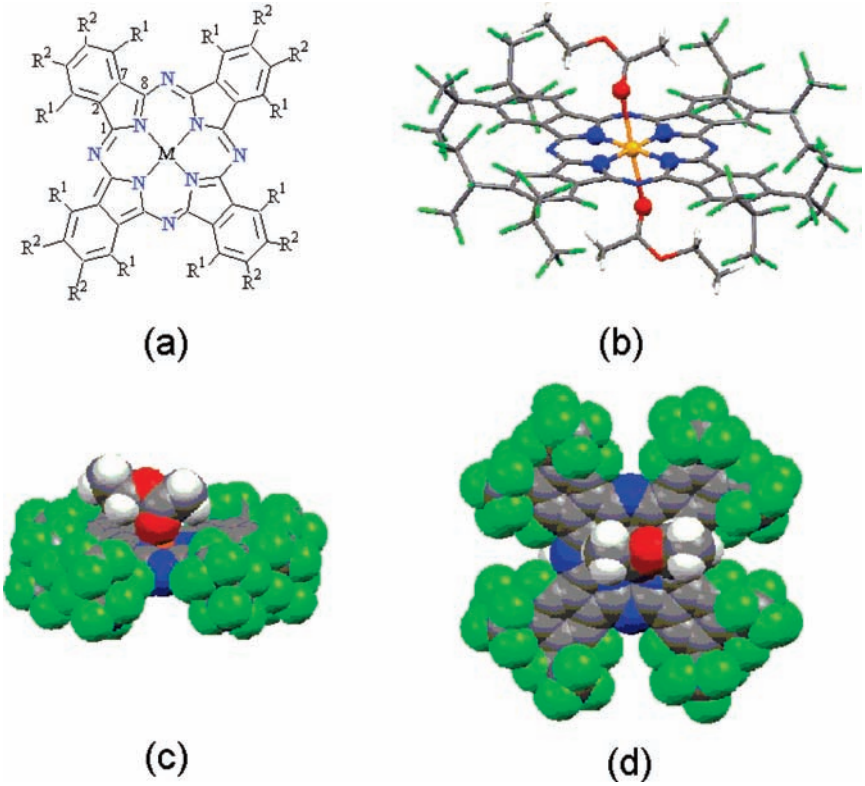

Figure 1. Crystal structures of F_{64}PcCu(ethyl acetate)$_2$. Color code: C, black; H, white; Cu, bronze; F, green; N, blue; O, red. (a) Structural formulas for H_{16}PcCu ($R^1 = R^2 = H$), F_{16}PcCu ($R^1 = R^2 = F$), and F_{64}PcCu ($R^1 = F$, $R^2 = CF(CF_3)_2$). (b) Ball and stick representation. Only the CuN_4O_2 chromophore is represented as spheres. (c) van der Waals representation viewed in the same orientation as in panel b. (d) van der Waals representation viewed perpendicular to the Pc ring.

molecules, namely, perfluoroalkylated perfluorophthalocyanines, exhibit enhanced solubility and favorable solid-state architectures that allow their atomic-level characterization via X-ray diffraction and lead as well to practical applications in catalysis, photophysics, and photodynamic therapy. The X-ray structure of F_{64}PcM (M = 2H, Zn, Co) revealed that the F_{64}Pc ring retains its planarity.[2,4,5] Vapor deposition of different metal F_{64}Pc's led to intensely colored thin films with an almost negligible extent of intermolecular electronic coupling,[7] a favorable property for heterogeneous and homogeneous catalysis applications.

In view of the potential catalytic and other applications of R_f-substituted Pc's, their electronic structures are of interest. In particular, open-shell molecules exhibit electronic and spin density distributions that could be probed via magnetic resonance techniques. In the present work, we compare the properties of F_{64}PcCu with those of other Cu(II) phthalocyanines. For this series, the variable parameter is the nature of the peripheral groups, while the metal is a constant. Axial ligation is also considered.

F_{64}PcCu is found to be moderately soluble in alcohols, which has important implications for its potential applications. Besides ^{19}F NMR, X-ray diffraction, and magnetic measurements, we use a combination of continuous-wave electron paramagnetic resonance (CW EPR), electron spin echo envelope (ESEEM), and pulsed electron nuclear double resonance (ENDOR) techniques to characterize F_{64}PcCu in the solid phase and in an ethanol solution. Although X-band (9.5 GHz) CW EPR methods have been used extensively to investigate metal phthalocyanines,[8−13] the application of high-field EPR[14,15] or ESEEM and ENDOR techniques[16−19] to these systems is still quite limited. Some of us showed in earlier work the strength of the latter EPR methods to detect the subtle effects of the matrix and peripheral substituents on the electronic structure of PcM's

(3) Minnes, R.; Weitman, H.; Lee, H.-J.; Gorun, S. M.; Ehrenberg, B. *Photochem. Photobiol.* **2006**, *82*, 593–599.
(4) Bench, B. A.; Beveridge, A.; Sharman, W. M.; Diebold, G. J.; van Lier, J. E.; Gorun, S. M. *Angew. Chem., Int. Ed.* **2002**, *41*, 748–750.
(5) Bench, B. A.; Brennessel, W. W; Lee, H.-J.; Gorun, S. M. *Angew. Chem., Int. Ed.* **2002**, *41*, 750–754.
(6) Keizer, S. P.; Mack, J.; Bench, B. A.; Gorun, S. M.; Stillman, M. J. *J. Am. Chem. Soc.* **2003**, *125*, 7067–7085.
(7) Keil, C.; Tsaryova, O.; Himcinshi, C.; Wöhrle, D.; Hild, O. R.; Zahn, D. R. T.; Gorun, S. M.; Schlettwein, D. *Thin Solid Films* **2009**, *517*, 4379–4384.
(8) Guzy, C. M.; Raynor, J. B.; Symons, M. C. R. *J. Chem. Soc. A.* **1969**, 2299.
(9) Abkowitz, M.; Chen, I.; Sharp, J. H. *J. Chem. Phys.* **1968**, *48*, 4561.
(10) Graczyk, A.; Dobkowski, J. *J. Magn. Reson.* **1979**, *34*, 467–474.
(11) Gardberg, A. S.; Doan, P. E.; Hoffman, B. M.; Ibers, J. A. *Angew. Chem., Int. Ed.* **2001**, *40*, 244–246.
(12) Thompson, J. A.; Murata, K.; Durcharne, R.; Poirier, M.; Hoffman, B. M. *Phys. Rev. B* **1999**, *60*, 523–529.
(13) Sharoyan, E. G.; Manukyan, A. S *J. Porphyrins Phthalocyanines* **2005**, *12*, 846–851.
(14) Krzystek, J.; Pardi, L. A.; Brunel, L.-C.; Goldberg, D. P.; Hoffman, B. M.; Licoccia, S.; Telser, J. *Spectrochim. Acta, Part. A* **2002**, *58*, 1113–1127.
(15) Krzystek, J.; Telser, J.; Pardi, L. A.; Goldberg, D. P.; Hoffman, B. M; Brunel, L.-C. *Inorg. Chem.* **1999**, *38*, 6121–6129.
(16) Finazzo, C.; Calle, C.; Stoll, S.; Van Doorslaer, S.; Schweiger, A. *Phys. Chem. Chem. Phys.* **2006**, *8*, 1942–1953.
(17) Finazzo, C.; Van Doorslaer, S.; Schweiger, A. *J. Porphyrins Phthalocyanines* **2003**, *7*, 89–96.
(18) Greiner, S. P; Rowlands, D. L; Kreilick, R. W *J. Phys. Chem.* **1992**, *96*, 9132–9139.
(19) Fukui, K.; Ohya-Nishiguchi, H.; Kamada, H.; Iwaizumi, M.; Xu, Y. *Bull. Chem. Soc. Jpn.* **1998**, *71*, 2787–2796.

(M = Cu, Co).[16] It has been shown in recent years that EPR studies benefit from density functional theory (DFT) computations of the spin-Hamiltonian parameters of the system under study.[20] In this report, we compare the outcome of the DFT computations of $F_{64}PcCu$ not only with the experimental EPR data, but also with the X-ray and ^{19}F NMR data, revealing essential points of its electronic structure. EPR and X-ray data confirm the ability of $F_{64}PcCu$ to axially ligate different molecules in the solid phase and in solution. This ligation and the overall packing have a marked influence on the magnetic characteristics of the powders.

Materials and Methods

Materials. All reagents were obtained from commercial sources and used without purification, unless stated otherwise. Isotopically enriched solvents (99%) were obtained from Cambridge Isotopes Laboratories.

Synthesis of 1,4,8,11,15,18,22,25-Octafluoro-2,3,9,10,16,17,23,24-octakis-perfluoro-isopropyl Copper(II) Phthalocyanine, $F_{64}PcCu$. Perfluoro-(4,5-di-isopropyl)phthalonitrile[21] (0.1 g, 0.2 mmol), and $Cu(CH_3COOH)_2 \cdot H_2O$ (0.02 g, 0.1 mmol) were mixed with 5 mL of freshly distilled nitrobenzene under a nitrogen atmosphere and heated gradually to 200 °C. After 4 h, the solvent was removed under reduced pressure and the crude product was chromatographed on silica gel to give 0.022 g of $F_{64}PcCu$ (21% yield). ^{1}F-NMR (300 MHz, d_6-acetone, C_6F_6 std): $\delta = -69.97$ (CF_3, 48F), -107.28 (aromatic F, 8F), -164.20 (aliphatic F, 8F). UV−vis (EtOH, 1×10^{-5} mol/L) λ nm (log ε): 681 (5.4), 613 (4.67), 383 (4.8). EI-MS (200 °C, 70 eV): m/z 2063 [M^+]. IR (KBr): ν = 2929, 1597, 1507, 1454, 1286, 1247, 1219, 1169, 1104, 984, 967, 752, 730 cm^{-1}. Single-crystals suitable for X-ray crystallography were obtained from ethyl acetate (EtOAc) by slow evaporation in air. The solution used for evaporation was prepared by first obtaining a saturated solution, filtering it to remove any solid, and then adding another 25% by volume of pure ethyl acetate.

An alternative preparation using microwave radiation was reported recently.[7] An improved variation is reported here. A mixture of perfluoro-(4,5-di-isopropyl)phthalonitrile (0.5 g, 1 mmol) and $Cu(CH_3COO)_2 \cdot H_2O$ (0.1 g, 0.5 mmol) was heated to 190 °C for 12 min. After forced cooling with air, the resulting crude product was washed with hot toluene and acetonitrile to remove brown and yellow impurities. The pure complex was obtained in 48% yield upon further chromatographic purification on silica gel using a 1:1 EtOAc/hexane mixture.

For solution EPR measurements, solvent-free $F_{64}PcCu$ was dissolved in ethanol, deuterated ethanol-d_6, or ^{13}C-labeled ethanol to a concentration of $\sim 1 \times 10^{-3}$ M.

Methods. Mass spectra were recorded at the University of Michigan Mass Spectrometry facilities. ^{19}F NMR spectra were recorded using a Bruker 300 MHz instrument. Magnetic measurements were performed using a Quantum Design SQUID magnetometer, MPMS-XL, between 5 and 300 K. Single-crystal X-ray data were collected on a Bruker SMART CCD diffractometer equipped with a variable-temperature nitrogen cold stream using graphite-monochromated Mo Kα radiation (λ = 0.710 73 Å). Computations were carried out using the *SHELXTL* package.[22] Further information can be found in the Supporting Information.

X-band continuous-wave (CW) EPR spectra were recorded with a Bruker ESP300E spectrometer (microwave (mw) frequency 9.43 GHz) equipped with a gas-flow cryogenic system, enabling operation from 2.5 K to room temperature. The spectra were recorded with a mw field modulation of 0.5 mT and 100 kHz modulation frequency. The magnetic field was calibrated with an NMR Gaussmeter (Bruker ER 035M). X-band pulsed EPR and ENDOR (electron nuclear double resonance) experiments were performed using a Bruker ESP380E spectrometer (9.76 GHz) equipped with a liquid He cryostat from Oxford, Inc. All experiments were performed at T = 10 K, using a repetition rate of 1 kHz. The magnetic field was measured with a Bruker ER 035M NMR Gauss meter.

Davies-ENDOR experiments[23] were performed using the mw pulse sequence $\pi - T - \pi/2 - \tau - \pi - \tau -$echo with $t_{\pi/2}$ = 24 ns, t_π = 48 ns, T = 7.4 μs, and τ = 176 ns. An rf pulse of variable frequency and length 5.4 μs was applied during time T. The rf increment was set to 100 kHz.

Mims-ENDOR spectra[24] were recorded with an mw pulse sequence $\pi/2 - \tau - \pi/2 - T - \pi/2 - \tau -$echo with $t_{\pi/2}$ = 16 ns and T = 14 μs. The τ value was changed from 88 to 216 ns in steps of 32 ns, and the corresponding spectra were summed to avoid blind spots in the spectrum. An rf pulse of 11 μs with variable frequency was applied during the time interval T with an rf increment of 50 kHz.

The HYSCORE (hyperfine sublevel correlation) spectra[25] were measured using a pulse sequence $\pi/2 - \tau - \pi/2 - t_1 - \pi - t_2 - \pi/2 - \tau -$echo, with pulse lengths $t_{\pi/2} = t_\pi$ = 16 ns. Two τ values (96 and 176 ns) were used, and the corresponding spectra were added together in the frequency domain after normalizing to the noise level to avoid blind spots. The time intervals t_1 and t_2 were varied from 96 to 5696 ns in steps of 16 ns. An eight-step phase cycle was used to eliminate unwanted echoes.

The W-band (94 GHz) ESE (electron spin echo)-detected EPR experiments[26] were performed on a Bruker ELEXSYS E680 spectrometer in conjunction with a split-coil Oxford 6T superconducting magnet equipped with an Oxford flow cryostat and a Bruker cylindrical cavity. The experiments were performed at 4.5 K with an mw pulse sequence $\pi/2 - \tau - \pi - \tau -$echo with $t_{\pi/2}$ = 140 ns, t_π = 280 ns, and τ = 748 ns.

EPR Data Processing. All CW-EPR and Davies- and Mims-ENDOR spectra were simulated using the EasySpin package.[27] The HYSCORE data were processed with MATLAB 7 (MathWorks, Inc., Natick, MA). The time traces of the HYSCORE spectra were baseline corrected with a third-order polynomial, apodized with a Hamming window and zero filled. After a two-dimensional Fourier transformation, the absolute value spectra were calculated. The HYSCORE spectra were simulated using a program developed at ETH Zurich.[28]

X-ray Data Collections and Processing. Several crystals, obtained from ethanol and ethyl acetate, exhibited severe twinning with multiple domains. Several structural analyses yielded R values of 8% or above confirming only the atomic connectivity and revealing the rough features of the solid-state packing.[7]

The data reported here were obtained from a thin, ~0.1 mm slice, obtained by cutting a regular crystal to give a prism-shaped crystal of dimensions $0.37 \times 0.36 \times 0.11$ mm^3. The specimen represents mostly a single domain and thus simplified the X-ray analysis. Cell parameters were determined from a nonlinear least-squares fit of 6520 peaks in the range $2.25° < \theta < 25.23°$. A total of 63 099 data were measured in the range $2.03° < \theta < 25.00°$ using ω oscillation frames. The data were corrected for

(20) Neese, F. *Coord. Chem. Rev.* **2009**, *253*, 526–563.
(21) Gorun, S. M.; Bench, B. A.; Carpenter, G.; Beggs, M. W.; Mague, J. T.; Ensley, H. E. *J. Fluorine Chem.* **1998**, *91*, 37–40.
(22) Sheldrick, G. M. *SHELXTL*, version 6.14; Bruker AXS, Inc.: Madison, WI, 2004.
(23) Davies, E. R. *Phys. Lett.* **1974**, *A47*, 1–2.
(24) Mims, W. B. *Proc. R. Soc.* **1965**, *283*, 452.
(25) Höfer, P.; Grupp, A.; Nebenführ, H.; Mehring, M. *Chem. Phys. Lett.* **1986**, *132*, 279–282.
(26) Schweiger, A.; Jeschke, G. *Principles of Pulse Electron Paramagnetic Resonance*; University Press Oxford: Oxford, U.K., 2001.
(27) Stoll, S.; Schweiger, A. *J. Magn. Reson.* **2006**, *178*, 42–55.
(28) Madi, Z. L.; Van Doorslaer, S.; Schweiger, A. *J. Magn. Reson.* **2002**, *154*, 181.

absorption by the semiempirical method[29] giving minimum and maximum transmission factors of 0.834 and 0.949. The data were merged to form a set of 13 451 independent data with $R(\text{int}) = 0.0925$ and a coverage of 99.5%. The monoclinic space group $P2_1/n$ was confirmed by systematic absences and statistical tests and verified by subsequent refinement. The structure was solved by direct methods and refined by full-matrix least-squares methods on F^2. Hydrogen atom positions were initially determined by geometry and refined using a riding model. Non-hydrogen atoms were refined with anisotropic displacement parameters. Hydrogen atom displacement parameters were set to 1.2 (1.5 for methyl) times the displacement parameters of the atoms to which they are bonded. A total of 1303 parameters were refined against four restraints and 13 451 data to give $wR(F^2) = 0.1615$ and GOF = 1.004 for weights of $w = 1/[\sigma^2(F^2) + (0.0868P)^2]$, where $P = [F_o^2 + 2F_c^2]/3$. The final $R(F)$ was 0.0583 for the 8564 observed, $[F > 4\sigma(F)]$, data. The largest shift/s.u. was 0.020 in the final refinement cycle. The final difference map had maximum and minimum electron densities of 2.259 and -0.569 e/Å^3, respectively. The maximum peak of 2.259 e/Å^3 height is believed to be the representation of the metal from a very minor twin domain, which was still present in the cut crystal.

DFT Computations. Spin-unrestricted DFT computations were performed with the ORCA package (version 2.7.β)[30−34] on different F_{64}PcCu and F_{64}PcCu(ethanol)$_2$ models and the diamagnetic F_{64}PcZn(ethanol)$_2$. Model A is F_{64}PcCu in vacuum, model B is F_{64}PcCu in ethanol, model C is F_{64}PcCu-(ethanol)$_2$ in vacuum, and model D is F_{64}PcCu(ethanol)$_2$ in ethanol. To simulate the solvent, a dielectric surrounding with the dielectric constant of ethanol according to the COSMO model[35] is used.

For the geometry optimizations, the Becke−Perdew density functional (BP86)[36−38] was used together with the resolution of the identity method.[39−41] The split-valence plus polarization (SV(P)) basis set[42,43] was used for all atoms except for the copper and zinc atom a more polarized triple-ζ valence (TZVPP) basis[42,43] was used. The energy was converged to 1×10^{-8} hartree (E_h), and the convergence tolerances in the geometry optimization were 3×10^{-4} E_h/bohr for the gradient and 5×10^{-6} E_h for the total energy. The coordinates of the optimized structures are given in the Supporting Information.

Single-point calculations with the B3LYP[44] functional and using the optimized geometries were carried out to predict the EPR and NMR spectral parameters. In these calculations, the same basis sets were used as in the geometry optimization except for the copper basis, which was the triply polarized "Core Properties" (CP(PPP))[45,46] basis. For the zinc atom, the TZVPP basis was used. For the isoindole nitrogen atoms, the pyrrole carbon atoms, and the two closest hydrogen atoms, the Barone "EPR-II" basis set[47] was used.

Results and Discussions

The classical procedure for synthesizing phthalocyanines includes prolonged heating periods in high boiling solvents. Microwave-assisted heating technology often results in shortened reaction times and less impurities, as shown for the fluorinated materials too.[7] The volatility of the perfluorinated precursors, however, is an issue; thus good mixing in sealed chambers is a requirement, often supplemented by the addition of a few drops of a solvent that also absorbs microwave radiation. The slightly higher yield reported here is an improvement, complemented by a more facile removal of impurities whose relative abundance turns out to be more sensitive to the reaction temperature than the yield.

The X-ray structure elucidation of the Cu complex proved to be a challenge due to the presence of multiple domains in most of the crystals. The final structure, obtained from a cut specimen, reveals the formation of the desired complex, F_{64}PcCu(ethyl acetate)$_2$. Atomic coordinates, bond distances, and angles are presented in Tables 1S−6S (Supporting Information). The ligand is planar, similar to F_{64}PcZn and Co complexes reported previously.[4,5] The metal is located at the geometric center of the four coordinating nitrogen atoms. Two ethyl acetate molecules axially coordinate the Cu, one being disordered (Figure 1b). The detailed geometry of the metal center is linked to the EPR studies and the DFT computations (*vide infra*). The Cu−N distances, which range from 1.952(3) to 1.963(3) Å, with an average of 1.958(3) Å, are statistically equivalent. The ethyl-acetate ligands are oriented along two collinear "grooves" of the complex, on opposite faces (Figure 1b,c,d). The "grooves" are spaces between the peripheral perfluoroalkyl groups, where the CH_3 groups of the ethyl moiety of the ethyl acetate can be accommodated with minimum steric hindrance. The CH_3 group of the acetate moiety is also located in the groove. The Cu−O (ester carbonyl group) distances are slightly different: Cu(1)−O(3F) = 2.515(4) Å, while Cu(1)−O(3E) = 2.537(4) Å. The shorter distance corresponds to the disordered ligand. The equatorial angles are normal, defining a square-planar geometry. The two oxygen atoms that complete the distorted octahedral coordination are tilted; the O−Cu−O bonds are almost collinear, making an angle of 176°. The least-squares vector through the O−Cu−O atoms makes a ∼77° angle with the Pc ring plane in the direction of the groove to which the ligand is aligned, 4° along the perpendicular direction. The tilt of the O−Cu−O vector is a bit puzzling since CuN_4O_2 chromophores prefer a Jahn−Teller distorted geometry of

(29) Sheldrick, G. M. SADABS. Program for Empirical Absorption Correction of Area Detector Data, University of Göttingen, Göttingen, Germany, 2007.
(30) Neese F., ORCA − an *ab initio*, density functional and semi empirical program package, University of Bonn, Bonn, Germany.
(31) Neese, F. *J. Chem. Phys.* **2001**, *115*, 11080–11096.
(32) Neese, F. *J. Phys. Chem. A* **2001**, *105*, 4290–4299.
(33) Neese, F. *J. Chem. Phys.* **2003**, *118*, 3939–3948.
(34) Neese, F. *J. Chem. Phys.* **2005**, *122*, 034107.
(35) Sinnecker, S.; Rajendran, A.; Klamt, A.; Diedenhof, M.; Neese, F. *J. Phys. Chem A* **2006**, *110*, 2235.
(36) Perdew, J. P. *Phys Rev. B* **1986**, *33*, 8822–8824.
(37) Perdew, J. P. *Phys Rev. B* **1986**, *34*, 7406–7406.
(38) Becke, A. D. *Phys. Rev. A* **1988**, *38*, 3098–3100.
(39) Dunlap, B. I.; Connolly, J. W. D.; Sabin, J. R. *J. Chem. Phys.* **1979**, *71*, 3396–3402.
(40) Vahtras, O.; Almlöf, J.; Feyereisen, M. W. *Chem. Phys. Lett.* **1993**, *213*, 514–518.
(41) The Ahlrichs auxiliary basis sets were obtained from the TurboMole basis sets library under ftp.chemie.uni-karlsruhe.de/pub/jbasen,Eichkorn, K.; Truetler, O.; Ohm, H.; Haser, M.; Ahlrichs, R. *Chem. Phys. Lett.* **1995**, *240*, 283.
(42) Schaefer, A.; Horn, H.; Ahlrichs, R. *J. Chem. Phys.* **1992**, *97*, 2571–2577.
(43) The Ahlrichs (2df,2pd) polarization functions were obtained from the TurboMole basis set library under ftp.chemie.uni-karlsruhe.de/pub/basen, Ahlrichs R. and co-workers (unpublished)
(44) Stephens, P. J.; Devlin, F. J.; Chabalowski, C. F.; Frisch, M. J. *J. Phys. Chem.* **1994**, *98*, 11623–11627.
(45) This basis is based on the TurboMole DZ basis developed by Ahlrichs and co-workers and obtained from the basis set library under ftp.chemie.uni-karlsruhe.de/pub/basen, Ahlrichs R.and co-workers (unpublished).
(46) The Ahlrichs polarization functions were obtained from the TurboMole basis set library under ftp.chemie.uni-karlsruhe.de/pub/basen, 2p functions from Wachters A. J. H. *Chem. Phys.*, **1970**, *52*, 1033 plus one f-function from the TurboMole library.
(47) Barone, V. In *Recent Advances in Density Functional Methods*; Chong, D. P., Ed.; World Scientific Publ. Co.: Singapore, 1996; p 287.

approximate D_{4h} point symmetry. While a solid state effect due to packing cannot be excluded completely, one can consider the effects of the carbonyl hybridization and steric hindrance. Thus, the ideal hybridization of the carbonyl oxygen requires a 120° Cu−O═C angle, which, if realized, will push either the CH_3- or the CH_3-CH_2- aliphatic groups too close to the π-macrocycle (Figure 1b,c,d). This steric hindrance can be alleviated by the opening of the Cu−O═C angles, which reach 146° and 151° and shift the coordinating oxygen atoms away from the perpendicular to the Pc ring. The final geometry allows the aliphatic backbone of the ester to be almost parallel to the Pc ring, thus minimizing its steric interaction with the macrocyle. This solid-state geometry, if it is indeed due mostly to intramolecular factors, is likely to be present in solution as well.

A geometric comparison with other PcCu molecules is limited due to the lack of structural information on the CuN_4O_2 chromophore. In general, there is a paucity of single-crystal structural information on Pc(−2)Cu(II) complexes, despite the fact that the parent molecule is industrially important as a polymorphic pigment. There are several structural determinations of the parent PcCu in the Cambridge Database (the β-polymorph). Out of the 10 known polymorphs,[48] additional powder X-ray structural and spectroscopic information are available for the α-, γ-, and ε-polymorphs.[49]

The medium-quality (R > 9%) X-ray structure of F_{16}PcCu has been very recently reported.[50] It exhibits the typical Herringbone-type architecture, albeit in the triclinic system. A direct comparison of bond distances of the two fluorinated Cu complexes, however, is hampered by the lower precision of the F_{16}Pc structure that exhibits estimated standard deviations (esd's) at the second decimal place. Structural and morphological transitions in solid-state F_{16}PcCu materials are common; in thin films they depend on the history of the sample and its thickness.[51] Apart from the parent molecule, a single additional type has been structurally characterized, namely, the octakis R-O,S (alkoxo, thioalkoxo)-substituted PcCu, with the substituents in the α (R^1 in Figure 1a) positions, as opposed to the β (R^2 in Figure 1a) positions we report here. The α positions are occupied by aromatic F in our case. Complexes with R = ethyl,[52] butyl,[53] isopentyl,[54] and benzyloxyethyl[55] have been reported. A bis-pyridine solvate has also been reported.[54b] Oxidized Pc rings[54c,d] are not included in the structural analysis.

There is no report in the CCDB (2010) of a β-substituted PcCu. The Cu−N distances reported thus far in the CCDB follow a binomial distribution with a set of distances around 1.94 Å and another one around 1.995 Å (Figure S5 (Supporting Information)). The first set comprises only powder data for the four-coordinated α and γ polymorphs of PcCu[48] as well as two of the distances of the six-coordinated complex.[54b] The second set contains the remaining four-coordinated PcCu structures including the alkoxo-substituted ones.[52,53,54a,b] The average Cu−N distance reported here, 1.958(3) Å, is within the range observed for four-coordinated structures despite belonging to a six-coordinated complex. These data thus suggest weak axial coordination, not surprising for the ester ligand. The fact that a weakly coordinated ligand binds at all, is attributed to the very high electronic deficiency of the metal center imparted by the fluorinated groups, as opposed to solid-state effects (stacking), as evidenced for F_{16}PcCu. Solution studies, *vide infra*, confirm that weakly bonding ligands remain coordinated in solution.

The way the F_{64}PcCu(ethyl acetate)$_2$ molecules are organized in solid state is important. The polymorphs of the parent PcCu ($R^1 = R^2 = H$, M = Cu in Figure 1a) exhibit different colors, important for the dye industry and other applications. The variable packing of the molecules results in variable $\pi-\pi$ interactions that alter the energy of the frontier orbitals, a phenomenon that could also result in orientation-dependent ionization potentials of PcCu films.[56]

The aggregation in the solid state is dependent upon the peripheral ligands and the presence of axial ligands. Figure 2 depicts the packing diagrams for F_{64}PcCu viewed along the three crystallographic axes.

The packing diagrams reveal a columnar arrangement of similarly oriented molecules, clearly different from the common herringbone pattern observed for β-PcCu and F_{16}PcCu, but somewhat similar to the structure of α-PcCu.[48] In F_{64}PcCu(ethyl acetate)$_2$, however, the molecules in each column are offset by ∼8 Å. In the α-PcCu polymorph, the nearest intermolecular Cu···Cu and Pc···Pc contacts are at 3.8 and 3.4 Å, respectively. The same distances for F_{64}PcCu(ethyl acetate)$_2$ are 9.2 and 12.2 Å, respectively. The differences, undoubtedly due to the presence of both axial ligands and bulky peripheral groups in F_{64}PcCu(ethyl acetate)$_2$, underscore the site isolation of the metal centers and suggest that the paramagnetic centers are magnetically diluted in the solid state and in solution, as revealed in the EPR experiments (*vide infra*). The retention of axial ligand(s) in solution, favored by the high Lewis acidity of the metal, could be an important contributing factor resulting in the hindering of the electronic and magnetic communications between the paramagnetic metal centers.

DFT calculations of F_{64}PcCu were performed in order to provide a better understanding of its electronic structure and associated magnetic resonance parameters. The minimized structure was compared with the X-ray geometry by least-squares overlapping the experimental and theoretical structures, Figure 3.

The overlap of the metalated Pc macrocycles and the atoms directly linked to the aromatic ring is excellent as judged by the equivalent 5% discrepancy factor between calculated and observed values. There are small discrepancies in the

(48) Erk, P.; Hengelsberg, H.; Haddow, M. F.; van Gelder, R. *CrystEngComm* **2004**, *6*, 474–483.
(49) Achar, B. N.; Lokesh, K. S. *J. Solid State Chem.* **2004**, *177*, 1987–1993.
(50) Yoon, S. M.; Song, H. J.; Hwang, I.; Kim, K. S.; Choi, H. C. *Chem. Commun.* **2010**, *46*, 231–233.
(51) Yang, J. L.; Schumann, S.; Jones, T. S. *J. Phys. Chem. C* **2010**, *114*, 1057–1063.
(52) Lin, M.-J.; Wang, J.-D.; Chen, N.-S. *Z. Anorg. Allg. Chem.* **2005**, *631*, 1352–1354.
(53) Cai, J.; Wang, J.; Huang, J.; Chen, N. *Chin. Sci. Bull.* **2002**, *47*, 644–646.
(54) (a) Lin, M.-J.; Wang, J.-D.; Chen, N.-S.; Huang, J.-L. *Z. Anorg. Allg. Chem.* **2006**, *632*, 2315–2320. (b) Lin, M.-J.; Wang, J.-D.; Chen, N.-S.; Huang, J.-L. *J. Coord. Chem.* **2007**, *60*, 1479–1484. (c) $PcCu(SbF_6)_2$ is presumed to contain a doubly oxidized phthalocyanine ring: Gardberg, S.; Ibers, J. A. *Acta Crystallogr.* **2001**, *C57*, 528–529. (d) Related [PcC (ReO_4)] and [$PcCu(ReO_4)_2$] also containing oxidized Pc rings have been reported, see ref 11.
(55) Minch, B. A.; Xia, W.; Donley, C. L.; Hernandez, R. M.; Carter, C.; Carducci, M. D.; Dawson, A.; O'Brien, D. F.; Armstrong, N. R. *Chem. Mater.* **2005**, *17*, 1618–1627.
(56) Chen, W.; Huang, H.; Chen, S.; Huang, Y. L.; Gao, Y.; Wee, T. S. *Chem. Mater.* **2008**, *20*, 7017–7021.

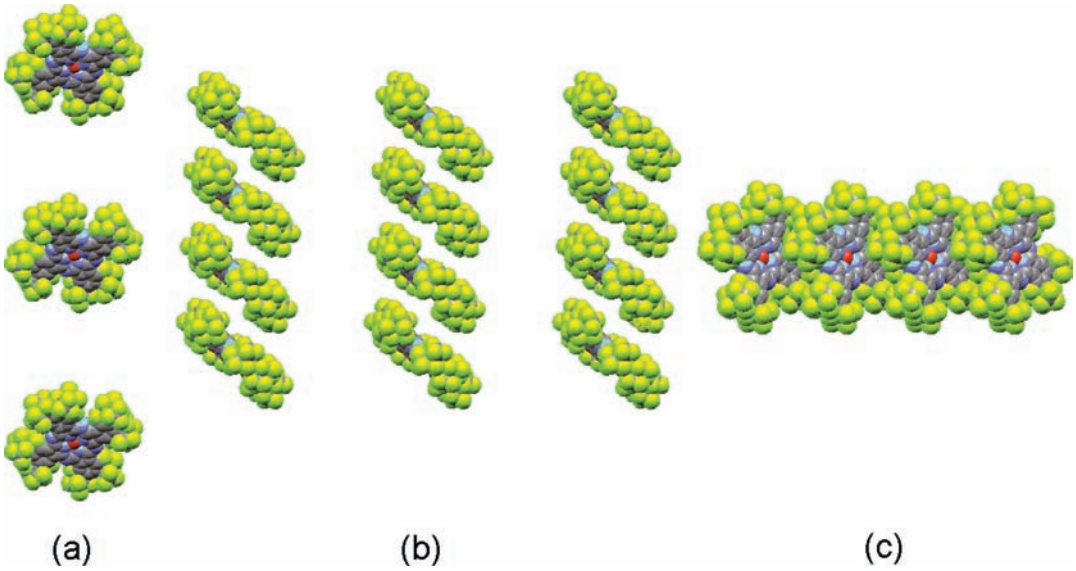

Figure 2. van der Waals packing diagrams for F_{64}PcCu viewed along the crystallographic *a*, *b*, and *c* axes. The axial ligands have been omitted for the sake of clarity.

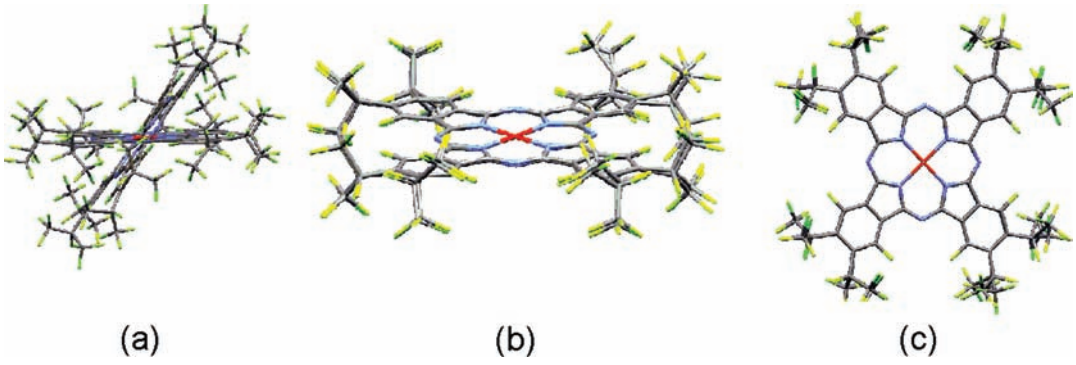

Figure 3. Overlay of the structures of F_{64}PcCu obtained via DFT calculations and single-crystal X-ray diffraction. The axially coordinated ethyl acetate ligands, revealed by the X-ray structure, have not been included in the calculations (model A) in order to verify the CuN_4-like coordination despite the presence of axial ligands (see text for details) and are thus omitted from the figure. (a) The two structures superimposed in arbitrary positions, but with the Cu ions as common point. (b) Overlap based on superposition of the aromatic macrocycles, side view. (c) View along the common 4-fold axis.

rotational orientation of the perfluoro-isopropyl groups, but such differences are expected considering that these groups are subject to intermolecular interactions in the solid state while the computations have been performed assuming a dielectric surrounding with the dielectric constant of ethanol (see further EPR results). From an electronic point of view, the orientation of the perfluoro-isopropyl groups is deemed to be virtually irrelevant under the reasonable assumption that the ring electronic structure is not affected by the R_f substituents orientation. This assumption is based upon the exclusive σ effect exerted by these groups, effects that are angular independent, in contrast to π effects. In this respect, the position of the aromatic F substituents, which participate in π back-bonding, are calculated correctly. In summary, the DFT computed structures are deemed accurate. The excellent geometrical agreement thus lends credence to the calculated electronic parameters, to be compared with those observed by magnetic resonance experiments, discussed next.

The room-temperature X-band CW-EPR spectra of a pure Pc^tCu (copper(II) 2,9,16,23-tetra-*tert*-butyl-29*H*,31*H*-phthalocyanine) powder are compared in Figure 4a,b with that of a pure F_{64}PcCu powder. While the spectrum of the former complex is characteristic of exchange-coupled Cu(II) complexes, the spectrum of the latter is characteristic of more isolated Cu(II) centers. A variable-temperature magnetic susceptibility study of F_{64}PcCu(ethyl acetate)$_2$ revealed a simple Curie behavior, that is, isolated paramagnetic species characterized by a spin-only value of their magnetic moment (Figure S6 (Supporting Information)). In contrast, the effective magnetic moments of parent PcCu polymorphs exhibit significant deviations from spin-only values. Specifically, the α-, β-, and ε-polymorphs exhibit higher than spin-only values, while the γ-polymorph exhibits a lower one.[49] Since (i) the oxidation level of Cu and its d^9 configuration is not in doubt and (ii) the $d_{x^2-y^2}$ nature of the singly occupied magnetic orbital is constant regardless of the polymorph, we conclude that intermolecular spin couplings are responsible for the observed variability of the magnetic properties of PcCu complexes. In the case of the γ-polymorph, the overall intermolecular magnetic interaction is antiferromagnetic, while for the other three polymorphs, it is ferromagnetic. This is reasonable considering that the polymorphs exhibit variable distances and angles between the $d_{x^2-y^2}$ magnetic orbitals, the two parameters that govern the sign and magnitude of intermolecular spin−spin couplings. Indeed, the molecular orientation could be very different. For example,

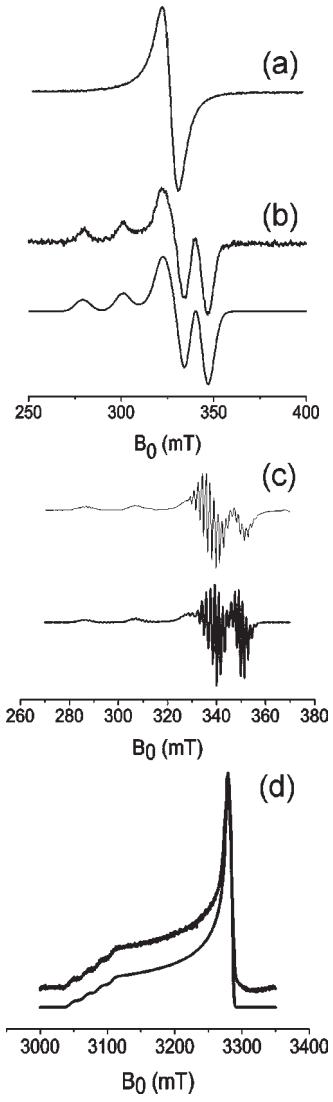

Figure 4. (a) Experimental X-band CW-EPR spectrum (9.43 GHz) of a pure Pc^tCu powder taken at RT with a microwave power of 2 mW. (b) Experimental X-band CW-EPR spectrum (9.43 GHz) of a pure $F_{64}PcCu$ powder taken at RT with a microwave power of 2 mW (top) and its simulation (bottom). (c) Experimental X-band CW-EPR spectrum (9.76 GHz) of a frozen ethanol solution of $F_{64}PcCu$ taken at 50 K with a microwave power of 0.28 mW (top) and its simulation (bottom). (d) Experimental (top) and simulated (bottom) W-band ESE-detected EPR spectrum of a frozen ethanol solution of $F_{64}PcCu$ taken at 4.5 K.

the α-polymorph has been shown by transmission electron diffraction to exhibit a molecular column stacking pattern[57] as opposed to the common herringbone-type molecular arrangement. In contrast, the metal centers in $F_{64}PcCu(ethyl\ acetate)_2$ and $F_{64}PcCu$ are magnetically isolated, the molecules being simple Curie paramagnets.

The lack of resolved copper and nitrogen hyperfine interactions in spectrum 4b is due to significant dipolar interaction between adjacent Cu(II) centers. The $F_{64}PcCu$ powder was subjected to X-band pulsed EPR experiments, but no spin echo could be observed, indicative of short phase-memory times, T_m. This observation confirms that the local concentration of paramagnetic spins is high, consistent with the properties of a normal powder (independent of stacking). The corresponding EPR parameters are listed in Table 1 and compared with other similar systems. The sign of the copper hyperfine values is set negative in accordance with earlier studies on copper complexes.[16,58]

In order to study the electronic structure of $F_{64}PcCu$ in more detail using different EPR techniques, the complex was dissolved in an organic solvent. The X-band CW-EPR spectrum, Figure 4c, of its frozen ethanol solution is axially symmetric with resolved ^{63}Cu and ^{65}Cu hyperfine splittings ($I = {}^3/_2$). Additional splittings, due to the interactions of the unpaired electron with the four geometrically equivalent isoindole ^{14}N nuclei ($I = 1$) can be observed. Since small rhombicities of the **g** matrix may not be resolved at the standard X-band frequency, a W-band ESE-detected EPR spectrum was recorded. This spectrum, Figure 4d, confirms the axiality of the **g** matrix. Upon dissolution of the $F_{64}PcCu$ powder in ethanol, the principal g values increase and the $|A_{\|}|$ value decreases. A similar trend is found when the EPR values of CuPc magnetically diluted in H_2Pc and dissolved in H_2SO_4 are compared (Table 1). This variation suggests a ligation effect by the solvent molecules, although a pure matrix polarity effect cannot be excluded at this stage. The DFT computations qualitatively predict the same trend when the $F_{64}PcCu$ and $F_{64}PcCu(ethanol)_2$ models in vacuum and in ethanol are compared (Table 1).

In order to determine the hyperfine and nuclear quadrupole principal values of the isoindole nitrogen atoms of $F_{64}PcCu$ in ethanol, X-band Davies ENDOR spectra were recorded at different observer positions (Figure 5). From the simulation of these spectra (Figure 5), the set of hyperfine and nuclear quadrupole values listed in Table 2 was obtained.

Note that the Q_z component (aligned along the Pc normal) equals 0 within experimental errors. The ^{14}N hyperfine values were used to refine the simulations of the CW-EPR spectrum in Figure 4 (principal g and A^{Cu} values given in Table 1). In the Davies-ENDOR spectrum, taken at a magnetic field setting corresponding to $g = g_{\perp}$, a broad signal is observed between 30 and 35 MHz, stemming from the copper hyperfine interaction. Although it is not possible to derive the exact in-plane copper hyperfine and nuclear quadrupole values from this broad signal, it does put a further constraint on the possible A^{Cu} values. The experimental ^{14}N principal hyperfine values are close to those observed for PcCu and Pc^tCu in H_2SO_4. These values are lower than the ones observed for PcCu and Pc^tCu in nonpolar environments (Table 1). A similar trend is also predicted by the DFT computations for $F_{64}PcCu$ and $F_{64}PcCu(ethanol)_2$. The DFT computations also predict a Q_z component that is close to 0 in the case of ethanol ligation.

In order to verify the previous suggestion of ethanol coordination to $F_{64}PcCu$, X-band ^1H HYSCORE spectra of a frozen ethanol solution of $F_{64}PcCu$ were taken at different observer positions (Figure 6).

For all observer positions, a clear ridge around the proton Larmor frequency is visible, a ridge that disappears upon deuteration of the solvent (Supporting Information, Figure S7). The proton HYSCORE signals can be simulated using a proton hyperfine tensor with principal values $A_x = -2.1$ MHz, $A_y = -2.1$ MHz, $A_z = 4.4$ MHz, and $\beta = 38°$ (the angle between the **g**- and ^{H}**A**-tensor) (Figure 6c,d). These values

(57) Hoshino, A.; Takenaka, Y.; Miyaji, H. *Acta Crystallogr.* **2003**, *B59*, 393–403.

(58) Valente, M.; Freire, C.; de Castro, B. *J. Chem. Soc., Dalton Trans.* **1998**, 1557–1562.

Table 1. Comparison of g and A^{Cu} Principal Values of $F_{64}PcCu$ with Those of Other Cu(II) Phthalocyanine Complexes[a]

	$g_\perp$	$g_\parallel$	$A_\perp$	$A_\parallel$	ref
Pc^tCu−toluene	2.0405	2.1625	−86	−643	16
$Pc^tCu-H_2SO_4$	2.0525	2.1994	−54	−608	16
$PcCu-H_2SO_4$	2.052	2.199	−52	−616	16
$PcCu-H_2Pc$ (1:500) powder	2.039	2.1577	−83	−648	16
$F_{64}PcCu$ powder	2.036[b]	2.165[b]	−80[c]	−645[c]	this work, EPR
$F_{64}PcCu$-ethanol	2.0484[d]	2.1855[d]	−61[e]	−620[e]	this work, EPR
$F_{64}PcCu$ (in vacuum; model A)	2.0411	2.1235	−7	−621	this work, DFT
$F_{64}PcCu$ (in ethanol; model B)	2.0422	2.1253	−2	−620	this work, DFT
$F_{64}PcCu(ethanol)_2$ (in vacuum; model C)	2.0483	2.1368	34	−601	this work, DFT
$F_{64}PcCu(ethanol)_2$ (in ethanol; model D)	2.0498	2.1393	43	−596	this work, DFT

[a] Hyperfine values are given in MHz for the ^{63}Cu isotope. The DFT computed values for the $F_{64}PcCu$ and $F_{64}PcCu(ethanol)_2$ models are also given. Full computational details are presented in the Supporting Information. [b] Experimental error = 0.001. [c] Experimental error = 5 MHz. [d] Experimental error = 0.0003. [e] Experimental error = 3 MHz.

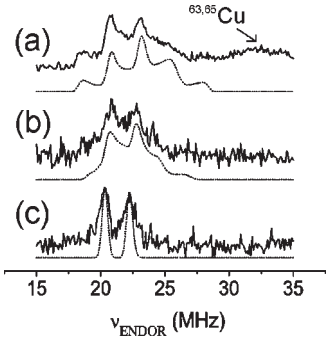

Figure 5. Experimental and simulated X-band nitrogen Davies-ENDOR spectra of a frozen ethanol solution of $F_{64}PcCu$ for observer positions (a) $g = g_\perp$ (B_0 = 340.0 mT), (b) B_0 = 318.0 mT, and (c) $g = g_\parallel$, $m_I = -^3/_2$ (B_0 = 292.0 mT).

agree with the proton hyperfine coupling predicted for the hydroxyl proton of the ligating ethanol molecules in model D ($^H\mathbf{A}$ = [−2.3 −2.3 4.1] MHz), confirming the ligation of ethanol. Model C gives similar results (see Supporting Information, Table 8S). DFT computations predict smaller hyperfine couplings for the alkyl protons of the coordinating ethanol (Supporting Information, Table 8S). HYSCORE simulations (not shown) indicate that these couplings contribute mainly to the central signal around the Larmor frequency and do not alter the overall shape of the HYSCORE ridge. In agreement with the XRD finding for $F_{64}PcCu(ethyl\ acetate)_2$, we assume that a double ligation of ethanol (overall six coordination) exists. The axiality of the **g** tensor (within the spectral resolution of the W-band EPR experiment) indicates that $F_{64}PcCu(ethanol)_2$ adopts a Jahn−Teller-type distorted geometry (strictly applicable only to $Cu(II)L_6$ chromophores) of approximate D_{4h} point symmetry. This feature is confirmed by the DFT calculations, which predict for model D an $O_{EtOH}-Cu-O_{EtOH}$ angle of 178.9° and a 94° angle of the O−Cu−O axis with the Pc plane in the direction of the groove to which the ligand is aligned. This observation indicates that the experimental deviation from D_{4h} symmetry in the XRD structure of $F_{64}PcCu(ethyl\ acetate)_2$ is not present for the ethanol ligation and may be due to a packing effect in the crystal case.

Note that the maximum observed proton coupling stemming from the ethanol protons (4.4 MHz) is much larger than the maximum proton coupling observed for Pc^tCu in H_2SO_4 or toluene (~2 MHz) in agreement with the axial coordination of the −OH unit (and hence smaller H−Cu distance) in the former case. The distance between the copper nucleus and the hydroxyl proton is calculated using the point dipolar approximation as 3.2 ± 0.2 Å, assuming that all spin density is located on the copper nucleus. This value agrees with the one obtained from the optimized DFT geometry, 2.97 Å.

Unexpectedly, signals stemming from ^{13}C in natural abundance (1.1%) are observed in the low-frequency part of the HYSCORE spectrum taken at an observer position corresponding to $g = g_\perp$, Figure 7a. At this observer position, almost all orientations contribute to the spectrum: the $g_\parallel$, $m_I = {}^3/_2$ feature is quasi-coincidental with the $g_\perp$ feature at X-band, Figure 1c.

The ^{13}C HYSCORE signals could only be followed for a limited set of magnetic field settings and could be simulated using ^{13}C hyperfine couplings with a large isotropic coupling (two contributions: $^C\mathbf{A}_1 = \pm$[5.7 7.3 6.4] ± 0.5 MHz and $^C\mathbf{A}_2 = \pm$[3.4 7.4 2.7] ± 0.5 MHz) (Figure 7b). Control HYSCORE experiments were performed on a frozen ^{13}C-labeled ethanol solution of $F_{64}PcCu$ (Supporting Information, Figure S8). The ratio of the proton signal to the ^{13}C signal observed previously in the unlabeled solvent samples remained constant, the isotope labeling leading only to the appearance of a strong peak at the ^{13}C Larmor frequency stemming from the ^{13}C nuclei from the ethanol matrix. This observation proves that the strong ^{13}C couplings must stem from carbon atoms of the $F_{64}Pc$ ring. The carbon nuclei become observable despite the low abundance of the ^{13}C isotope, because of the high symmetry of the Pc ligand (several equivalent carbons contribute to the same signal) and favorable solubility. Note that such couplings have not been reported for other Cu(II) phthalocyanine complexes.

The DFT model D predicts ^{13}C hyperfine interactions $^C\mathbf{A}$ = [6.0 7.7 6.2] MHz for pyrrole carbons C1 and C8 and $^C\mathbf{A}$ = [4.9 7.7 3.0] MHz for pyrrole carbons C2 and C7 (see Figure 1a for numbering of the carbon atoms). Similar values were found for the equivalent carbons of the other three pyrrole rings, related by symmetry to the first set. These values agree very well with the observed couplings. All other carbons had much smaller couplings. Analogous results are found for DFT model C (Supporting Information, Table 8S).

Figure 8 shows the X-band fluorine Mims-ENDOR experiments of $F_{64}PcCu$ in frozen deuterated ethanol for different observer positions.

The maximum observed hyperfine coupling, 0.8 MHz, observed for the nonperipheral aromatic fluorine substituents is lower than the ones observed earlier for $F_{16}PcCu$, namely 1.3 MHz for the nonperipheral and 1.1 MHz for the peripheral fluorine atoms. The 0.5 MHz decrease in the

Table 2. Comparison of ^{14}N Hyperfine and Nuclear Quadrupole Parameters of the Isoindole Nitrogen Atoms for F_{64}PcCu in a Frozen Ethanol Solution and Other Phthalocyanine Complexes[a]

	A_x	A_y	A_z	Q_x	Q_y	Q_z	ref
Pc^tCu−toluene	56.4	44.8	45.7	−0.790	0.820	−0.030	16
$Pc^tCu-H_2SO_4$	52.4	41.2	41.8	−0.882	0.995	−0.113	16
$PcCu-H_2SO_4$	51.4	40.8	41.0	−0.878	0.998	−0.120	16
$PcCu-H_2Pc$ (1:500) powder	56.5	44.7	45.4	−0.760	0.765	−0.005	16
F_{64}PcCu−ethanol	52.2[b]	41.3[b]	42.7[b]	−0.9[c]	0.9[c]	0.0[d]	this work, ENDOR
F_{64}PcCu (in vacuum; model A)	60.1	47.3	48.6	−0.831	0.992	−0.161	this work, DFT
F_{64}PcCu (in ethanol; model B)	59.8	47.1	48.5	−0.871	0.996	−0.125	this work, DFT
$F_{64}PcCu(ethanol)_2$ (in vacuum; model C)	56.5	44.6	45.9	−0.988	1.032	−0.044	this work, DFT
$F_{64}PcCu(ethanol)_2$ (in ethanol; model D)	55.9	44.1	45.5	−1.022	1.038	−0.016	this work, DFT

[a] The x axis lies along the Cu−N bond, z lies along the normal of the phthalocyanine plane. All values are given in MHz. The experimental values are also compared with the values computed using DFT for different models. Full computational details are presented in the Supporting Information. [b] Experimental error = 0.2 MHz. [c] Experimental error = 0.2 MHz. [d] Experimental error = 0.1 MHz.

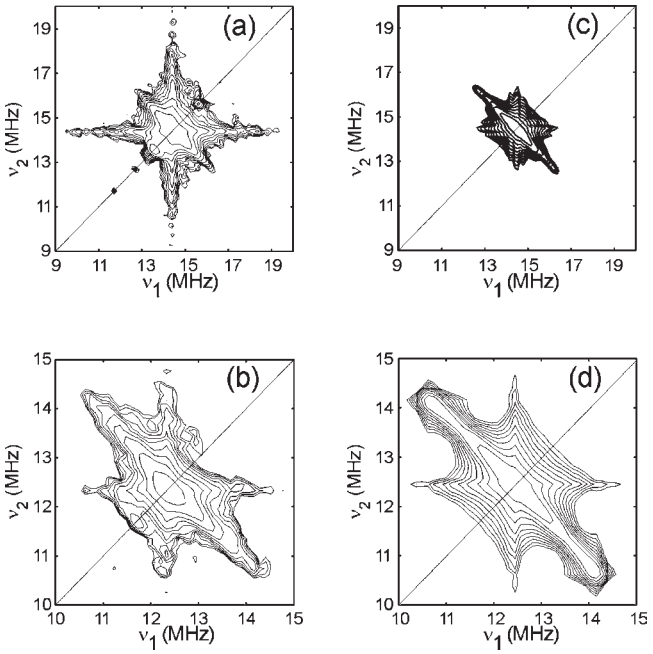

Figure 6. Experimental (a,b) and simulated (c,d) X-band proton HYSCORE spectra of a frozen ethanol solution of F_{64}PcCu. The spectra were recorded for observer positions (a) $g = g_\perp$ (B_0 = 338.2 mT) and (b) g = $g_\parallel$, $m_I = -3/2$ (B_0 = 290.0 mT). The simulation parameters are given in the text.

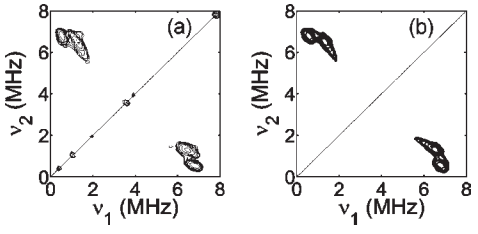

Figure 7. Experimental (a) and simulated (b) X-band ^{13}C HYSCORE spectra of a frozen ethanol solution of F_{64}PcCu recorded for observer position corresponding to $g = g_\perp$.

hyperfine coupling of the nonperipheral fluorine atoms in F_{64}PcCu relative to those in F_{16}PcCu indicates a slight decrease of the spin density of the aromatic fluorine atoms in the former complex, probably due to the very strong electron-withdrawing effects of the aliphatic fluoroalkyl substituents.

From the Cu−F distances obtained for DFT model D, we can estimate the dipolar contribution to the ^{19}F hyperfine

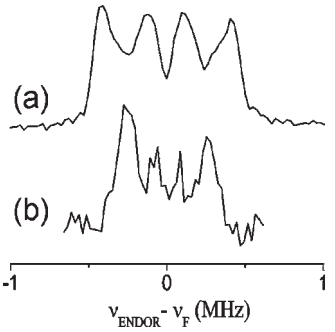

Figure 8. X-band fluorine Mims ENDOR spectra of a frozen ethanol solution of F_{64}PcCu. The spectra were recorded for observer positions (a) $g = g_\perp$ (B_0 = 341.6 mT) and (b) $g = g_\parallel$, $m_I = -3/2$ (B_0 = 291.5 mT).

tensors also taking the slight distribution of the spin density over the neighboring isoindole nitrogens into account. For the aromatic fluorine atoms, all located in nonperipheral positions, we find $\mathbf{T}_{dip} \approx$ [0.69 −0.34 −0.37] MHz (Cu−F = 6.02 Å). For the other ^{19}F nuclei, all aliphatic, we find an average distance of 8.82 Å, leading to $\mathbf{T}_{dip} \approx$ [0.22 −0.11 −0.12] MHz. The observed hyperfine interactions are thus predominantly dipolar in nature, a notion supported by the DFT data of model D, which predict maximum ^{19}F couplings of 1.0 MHz, while the isotropic hyperfine value varies between 0.005 and 0.08 MHz.

The ^{19}F NMR chemical shifts for the Cu complex are similar to those reported for the F_{64}PcZn complex [in brackets], despite the diamagnetism of the latter: δ = −69.97 [−71.3] (CF_3), −107.28 [−103.9] (aromatic F), −164.20 [164.6] (aliphatic F). The same results are obtained from the DFT calculations comparing the difference of the ^{19}F chemical shifts between the Cu and the Zn complex, $|\Delta\delta|$ = 0.6 ppm (CF_3), 0.4 ppm (aromatic F), and 0.5 ppm (aliphatic F). The negligible paramagnetic shift confirms the dominant dipolar interaction between the electron and the fluorine atoms and the negligible Fermi-contact contribution to the hyperfine values. A comparison with the aromatic F of F_{16}PcCu is not possible because its ^{19}F NMR does not appear to have been reported, probably due to its low solubility.

Figure 9a depicts $|^{Cu}A_\parallel|$ as a function of $g_\parallel$ for different copper phthalocyanine complexes revealing that the principal g and copper hyperfine values of Cu(II) phthalocyanines are predominantly determined by the matrix and less by the type of ring substituents. In earlier studies, the g and copper hyperfine values have been linked to the different

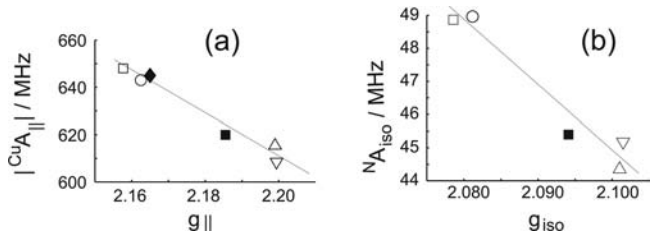

Figure 9. Correlation between (a) the copper $A_{||}$ values and the principal $g_{||}$ values and (b) the nitrogen A_{iso} and g_{iso} values for different Cu(II) phthalocyanines in different matrices: (○) Pc^tCu in toluene; (▽) Pc^tCu in H_2SO_4; (△) PcCu in H_2SO_4; (□) PcCu in H_2Pc powder; (◆) pure $F_{64}PcCu$ powder; (■) $F_{64}PcCu$ in ethanol.

Table 3. Parameters Derived from the EPR Data in Tables 1 and 2[a]

	κ	α^2	ρ^N	ref
Pc^tCu−toluene	0.310	0.729	0.0318	16
$Pc^tCu-H_2SO_4$	0.304	0.763	0.0293	16
$PcCu-H_2SO_4$	0.305	0.773	0.0289	16
$PcCu-PcH_2$ (1:500) powder	0.309	0.731	0.0318	16
$F_{64}PcCu$ powder	0.307	0.742		this work
$F_{64}PcCu$−ethanol	0.304	0.755	0.0295	this work

[a] $P\kappa$ = Fermi contact parameter, α^2 = covalency parameter, ρ^N = spin density on each of the isoindole nitrogen atoms.

ratios of σ and π bonding to the metal in the following way:[16,58]

$$A_{||} = P\left(-\kappa - \frac{4}{7}\alpha^2 + \Delta g_{||} + \frac{3}{7}\Delta g_{\perp}\right) \quad (1)$$

$$A_{\perp} = P\left(-\kappa + \frac{2}{7}\alpha^2 + \frac{11}{14}\Delta g_{\perp}\right) \quad (2)$$

where $\lambda = -830\ cm^{-1}$ is the spin−orbit coupling constant of the free copper(II) ion,[59] $-P\kappa$ is the Fermi contact parameter, $P = \beta_e\beta_n g_e g_n \langle r^{-3}\rangle = 1164$ MHz ($^{63}Cu(II)$)[59] is the dipolar hyperfine coupling parameter of the unpaired electron, $\Delta g_{||,\perp} = g_{||,\perp} - 2.0023$. Here α is the coefficient of the $d_{x^2-y^2}$ orbital in the b_{1g} orbital and thus α^2 can be viewed as a covalency parameter, describing the in-plane metal−ligand σ bonding. For a pure ionic binding, $\alpha^2 = 1$, for covalent binding $\alpha^2 < 1$. We notice a lower covalency of the copper−nitrogen bond in the more polar matrices (Table 3).

In this respect, it is interesting to note that Hoffman and co-workers reported $g_{||} = 2.16$ and $|^{Cu}A_{||}| = 575$ MHz for $[CuPc(ReO_4)_2]$.[11] The authors interpreted the similarity with the g and copper hyperfine values of CuPc as an indication that the energy separation between the $d_{x^2-y^2}$ and d_{xy} orbitals remains essentially the same after the double oxidation of the Pc ligand in Cu(II)Pc and axial coordination of two ReO_4^- ions. Comparison with Figure 9a shows that the $g_{||}$ and $A_{||}$ values of $[CuPc(ReO_4)_2]$ lie clearly below the currently found linear dependence, reflecting the change in the energy separation between the b_{1g} and b_{2g} orbitals due to the double oxidation.

The matrix influence is also noticeable when the apparent isotropic hyperfine values, $A_{iso} = (A_x + A_y + A_z)/3$, of the isoindole nitrogens are plotted versus $g_{iso} = (g_x + g_y + g_z)/3$, Figure 9b. Using the average Cu−N distance of 0.1958 nm from the XRD data, the point-dipolar contribution to the nitrogen hyperfine can be calculated[60] and the real isotropic part of the nitrogen hyperfine values, a_{iso}, can be determined as described in ref 16. For $F_{64}PcCu$ in ethanol, we find $a_{iso} = 45.42$ MHz. From this value, the spin density ($\rho_N = a_{iso}/a_0$ with $a_0 = 1538.22$ MHz[61]) can be calculated and compared with the one observed for other copper phthalocyanine complexes (Table 3). Again, the relative increase in the ionic character of the metal−N bond in $F_{64}PcCu$ is confirmed by the trend observed for ρ_N.

Although the current DFT computations reproduce the qualitative trends of the experimental observations quite well and the quantitative agreement with the experiment is satisfactory, there is not yet a perfect match. Present-day DFT methods are known to be problematic for computing the g and metal hyperfine values of transition metals.[20] The methods fail in calculating with high accuracy the indirect core level spin polarization, leading to false predictions of the Fermi contact term. Furthermore, the g-shift is systematically underestimated due to a combination of an overestimation of covalent bonding and too high d−d transition energies. Both trends are also observed here. In general, the agreement between theory and experiment for the hyperfine values of the ligand nuclei are better and can be used to evaluate the model at hand. In fact, the current-level DFT computations proved necessary and sufficient to interpret the ^{13}C hyperfine data. Moreover, the relatively good agreement between computation and experiment could be useful for comparing different DFT methods as well as for the future investigation of R_fPcM's with other substituents or metal centers, such as vanadium and cobalt. The deep understanding of the electronic and geometric features of the R_fPc-type complexes contributes to their evaluations for potential applications in optics, catalysis, and photocatalysis. Site isolation (single-site catalysts), for example, is an important parameter for designing efficient catalysts, while avoiding aggregation via tuning of the steric bulkiness of the metal complexes favors long-lived photoexcited states and thus the efficient production of singlet oxygen in particular and photocatalysis in general. Related R_fPc metal complexes, also easily soluble but with different d-orbital occupancies, are currently being studied in both solid state and solution to gain a deeper insight into their electronic structures and potential applications.

Conclusions

Here, we report on the first high-resolution single-crystal XRD structure of a β-substituted halogenated Cu phthalocyanine, namely, the perfluoroalkylated (R_f) phthalocyanine, $F_{64}PcCu$. This copper complex is remarkably soluble in environmentally friendly alcohols and other solvents due to its *iso*-C_3F_7 groups and axial ligation, in contrast to other reported copper phthalocyanines. X-ray diffraction studies prove that axial ligation of weakly coordinating ligands occurs, while the EPR studies show that the hexa coordination observed in the solid state is retained in solution. The coordination occurs despite the marked reduced covalency of

(59) Maroney, M. J.; Norman, J. G.; Osborne, J. H. *Inorg. Chem.* **1984**, *23*, 2261–2270.

(60) Hurst, G. C.; Henderson, T. A.; Kreilick, R. W. *J. Am. Chem. Soc.* **1985**, *107*, 7294–7299.

(61) Koh, A. K.; Miller, D. J. *Atom Data Nucl. Data* **1985**, *33*, 235–253.

the copper−nitrogen bond, as revealed by the EPR data and confirmed by the DFT studies. The enhanced Lewis acidity of the metal center imparted by the perfluoroalkyl substituents is most likely responsible for the stabilization of the additional axial binding. The DFT optimized geometries reproduce remarkably well the solid-state structure, lending credence to the solid-state results while also confirming the EPR parameters of F_{64}PcCu and F_{64}PcCu(ethanol)$_2$ observed experimentally as well as the associated trends linked to electronic structure tuning. Natural abundance ^{13}C hyperfine values are observed for the first time in copper phthalocyanines. Taken together, the DFT, ^{19}F NMR, and ^{19}F ENDOR data confirm that the Fermi contact contributions to the ^{19}F hyperfine couplings are negligible. Paramagnetic ^{19}F NMR signals are easily observable and magnetic susceptibility studies confirm the isolated nature of the paramagnetic centers. The current work outlines a detailed combined experimental and theoretical methodology that can be applied to gain deeper insights into the electronic and structural features of metallophthalocyanines.

Acknowledgment. This research was supported by FWO-Flanders (Grant G.0116.06, S.V.D.) and US Army (S.M.G.). H. M. thanks the University of Antwerp for Ph. D. funding. The authors are grateful to D. R. Powell for portions of the X-ray data.

Supporting Information Available: ORTEP representation at 50% probability level of the structure of F_{64}PcCu(ethyl acetate)$_2$, full packing diagram for F_{64}PcCu(ethyl acetate)$_2$, representation of the full structure of F_{64}PcCu(ethyl acetate)$_2$, full structure of F_{64}PcCu(ethyl acetate)$_2$ shown with the atoms represented as van der Waals spheres, histogram of Cu−N distances in Pc(2−)Cu(II) complexes (CCDB 2010), Curie plot for F_{64}PcCu in the solid state, crystallographic tables, geometries for the different DFT models for the F_{64}PcCu and F_{64}PcZn complexes, together with the coordinates of the atoms, computed hyperfine values for hydrogen nuclei and pyrrole carbon nuclei for models A−D, HYSCORE spectrum of a frozen deuterated ethanol solution of F_{64}PcCu, and HYSCORE spectrum of a frozen ^{13}C-labeled ethanol solution of F_{64}PcCu. This material is available free of charge via the Internet at http://pubs.acs.org.